

# Rotary Outliers and Rotary Offset Features in Large Language Models

André Jonasson<sup>1</sup>

## Abstract

Transformer-based Large Language Models (LLMs) rely on positional encodings to provide sequence position information to their attention mechanism. Rotary Positional Encodings (RoPE), which encode relative position by rotating queries and keys, have become widely used in modern LLMs. We study the features and patterns that emerge in queries and keys when using rotary embeddings. Our analysis reveals consistent patterns within the same model across layers and attention heads and across different models and architectures. We present and apply analysis techniques and show how the queries and keys use RoPE to construct various attention patterns, including attention sinks. We find and analyze outliers across models in queries and keys and find that they are likely to be found in rotary features with partial cycles. We derive bounds that tell us what rotary frequencies are likely to be selected as outlier features and at what minimum angle the query-key rotary pairs in these features tend to be above and verify the bounds empirically with models of significant architectural differences.

## 1. Introduction

Rotary positional embeddings (Su et al., 2024) have become a standard component in modern language models, yet their learned feature patterns remain poorly understood and are an active area of research (Barbero et al., 2024). While they have demonstrated strong performance across a range of model architectures and sizes, the underlying mechanisms by which they encode and utilize positional information are not well characterized.

In this paper, we analyze the internal representations of models using rotary positional embeddings (RoPE) to better understand how positional information is encoded and utilized. We find a heavy concentration of large magnitudes in the queries and keys at specific rotary features (see Figure

<sup>1</sup>Annokvick, Stockholm, Sweden. Correspondence to: André Jonasson <mail@andrejonasson.com>.

Preprint. Work in Progress.

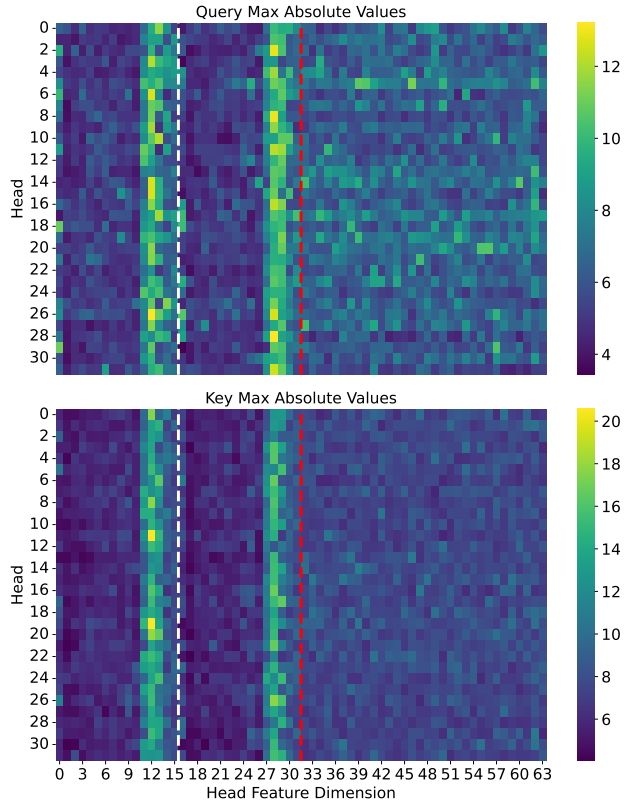


Figure 1. Maximum query and key absolute values across all layers in Phi-1. The white dashed line separates rotary (left) from non-rotary (right) features, we further separate the first dimensions of the rotary pairs (left) from the second dimensions (right) with a red dashed line. The two bands of large absolute values are located at the pair of rotary dimensions that are rotated by the same low frequencies in a sliced rotary implementation layout. See Appendix Figure 9 for mean magnitudes.

1). Through analysis and empirical validation, we derive and verify bounds that characterize these outlier features and their effects on attention scores.

These outlier features are particularly relevant in the context of model quantization. Work by (Dettmers et al., 2022) has shown that activation outlier features can significantly impact model performance during quantization. While their analysis focused primarily on activation outliers in additive positional encodings, similar outlier features exist for net-

works with rotary positional embeddings. The high-norm features we identify in rotary embeddings could affect the quantization errors for activation quantized models. This is because high-norm features tend to dominate the representation space, leading to larger quantization errors when the numerical precision is reduced. Furthermore, since keys are affected by these outliers, quantized key caches may require higher precision or more complex quantization algorithms (Liu et al., 2024b) to maintain model accuracy.

Throughout the analysis we choose to ignore all non-rotary features and focus solely on the rotary features. We analyze the features and patterns that emerge in queries and keys when using rotary embeddings and make the following contributions:

- We find outlier features appear in certain rotary frequencies across layers and heads within networks and that they exist across language models of different sizes and architectures.
- We show how a simple upper bound on the rotary frequency can be used to predict which frequencies are likely to contain outlier activations. This upper bound depends only on context length and rotary frequency.
- We derive a novel and simple lower bound for the query-key angles that also only depends on context length and rotary frequency. We demonstrate empirically that on average rotary outliers consistently operate within these bounds.
- We present other analysis on rotary features, such as the mechanism by which attention sinks often emerge from the rotary outlier features identified by our bounds.

## 2. Background

### 2.1. Attention Mechanism

The attention mechanism enables language models to dynamically focus on different parts of the input sequence (Vaswani, 2017). For sequence length  $n$ , attention operates on queries  $Q$ , keys  $K$ , and values  $V$  in  $\mathbb{R}^{n \times d}$ , computing:

$$\text{Attention}(Q, K, V) = \text{softmax}\left(\frac{QK^T}{\sqrt{d}} + M\right)V \quad (1)$$

where  $M$  is a causal mask ensuring each position only attends to previous tokens:

$$M_{ij} = \begin{cases} 0 & \text{if } i \geq j \\ -\infty & \text{otherwise} \end{cases} \quad (2)$$

Multi-head attention splits this computation into  $h$  parallel heads, each with dimension  $d_h = d/h$ :

$$\text{MultiHead}(Q, K, V) = \text{Concat}(\text{head}_1, \dots, \text{head}_h)W^O \quad (3)$$

where each  $\text{head}_i$  applies the attention mechanism to learned projections of  $Q$ ,  $K$ , and  $V$ . This structure allows the model to jointly attend to information from different representation subspaces (Vaswani, 2017).

### 2.2. Rotary Positional Embeddings

Rotary positional embeddings (Su et al., 2024) apply position-dependent rotations to queries and keys, by pairing features in the embedding and applying the same two-dimensional rotation to each pair. For position  $m$  and feature dimension  $i$ , the rotation matrix  $R_{\Theta}(m, i)$  is defined as:

$$R_{\Theta}(m, i) = \begin{bmatrix} \cos(m\theta_i) & -\sin(m\theta_i) \\ \sin(m\theta_i) & \cos(m\theta_i) \end{bmatrix} \quad (4)$$

where  $\theta_i = c^{-2i/d}$  controls the frequency for dimension  $i$ ,  $i$  ranges from 0 to  $\frac{r}{2}$  where  $r$  is the number of rotary feature dimensions, and  $c$  is a hyperparameter. Note that the step size  $\theta_i$  and frequency decrease as  $i$  increases. For query vector  $\mathbf{q}$  and key vector  $\mathbf{k}$  at position  $m$ , rotary embeddings transform pairs of features<sup>1</sup>:

$$\mathbf{k}_{m, \langle i \rangle} = \begin{bmatrix} k_{m, i} \\ k_{m, i + \frac{r}{2}} \end{bmatrix} \quad (5)$$

$$\text{RoPE}(\mathbf{k}_m)_i = R_{\Theta}(m, i)\mathbf{k}_{m, \langle i \rangle} \quad (6)$$

and similarly for  $\mathbf{q}$ , where  $\langle i \rangle$  denotes the  $i$ -th rotary pair. This rotation preserves the inner product structure while encoding relative positions. For queries and keys at positions  $m$  and  $n$  respectively, the inner product between their rotated features preserves relative position information:

$$\text{RoPE}(\mathbf{q}_m, m)_i^T \text{RoPE}(\mathbf{k}_n, n)_i \quad (7)$$

$$= \mathbf{q}_{m, \langle i \rangle}^T R_{\Theta}(m, i)^T R_{\Theta}(n, i) \mathbf{k}_{n, \langle i \rangle} \quad (8)$$

$$= (R_{\Theta}(m - n, i) \mathbf{q}_{m, \langle i \rangle})^T \mathbf{k}_{n, \langle i \rangle} \quad (9)$$

This shows that the inner product depends only on the relative position ( $m - n$ ) between the query and key, enabling the model to attend based on token distances. For networks with partial rotary embeddings, only a subset of the query and key feature dimensions receive rotations, with  $r < d$ .

The rotary embeddings enter into the attention mechanism by modifying the query-key dot products that determine

<sup>1</sup>Note that there are several possible layouts for RoPE.

attention weights. For a query  $\mathbf{q}_m$  at position  $m$  and key  $\mathbf{k}_n$  at position  $n$ , the dot product becomes:

$$\mathbf{q}_m^T \mathbf{k}_n = \sum_{i=1}^{r/2} (R_{\Theta}(m-n, i) \mathbf{q}_{m, \langle i \rangle})^T \mathbf{k}_{n, \langle i \rangle} \quad (10)$$

$$+ \sum_{i=r+1}^{d_h} q_{m, i} k_{n, i} \quad (11)$$

where the first sum is over rotary feature pairs and the second sum is over non-rotary features. The rotary features enable position-dependent attention through the rotation matrices  $R_{\theta}(n-m, i)$ , while non-rotary features contribute position-independent semantic matching. After scaling by  $1/\sqrt{d_h}$  and applying the causal mask, these modified dot products enter the softmax to produce attention weights:

$$\alpha_{mn} = \frac{\exp(\mathbf{q}_m^T \mathbf{k}_n / \sqrt{d_h} + M_{mn})}{\sum_{j=1}^n \exp(\mathbf{q}_m^T \mathbf{k}_j / \sqrt{d_h} + M_{mj})} \quad (12)$$

The attention weights  $\alpha_{mn}$  then combine the value vectors to produce the output. This mechanism allows the model to learn both position-aware and position-independent attention patterns through the selective use of rotary and non-rotary features.

### 3. Methodology

#### 3.1. Decomposing positional attention patterns

Instead of working with the  $n$  query and key vectors and  $n \times n$  dot products to understand the effect of the rotary features on the attention score, we simplify our analysis of the effect of the rotary features by working with the mean query and key vectors. For each rotary feature pair  $i$ , we can compute the dot product between the mean query and mean key vectors. We can then rotate the queries to get a sense for the evolution of the dot product contribution of the rotary feature pair with distance. Let  $\bar{\mathbf{q}}_{\langle i \rangle}$  be the mean query vector and  $\bar{\mathbf{k}}_{\langle i \rangle}$  be the mean key vector across all positions for rotary pair  $\langle i \rangle$ . We adopt the view that the query is incrementing its position  $p$  relative to the key and the key is stationary, which gives us the dot product per rotary feature pair:

$$d_i(p) = (R_{\Theta}(p, i) \bar{\mathbf{q}}_{\langle i \rangle})^T \bar{\mathbf{k}}_{\langle i \rangle} \quad (13)$$

$$= \|\bar{\mathbf{q}}_{\langle i \rangle}\| \|\bar{\mathbf{k}}_{\langle i \rangle}\| \cos(\phi_i + \theta_i p) \quad (14)$$

where  $\phi_i \in (0, 2\pi]$  is the initial counterclockwise angle between  $\bar{\mathbf{q}}_{\langle i \rangle}$  and  $\bar{\mathbf{k}}_{\langle i \rangle}$ . This gives us an  $\frac{\pi}{2}$ -dimensional vector function  $\mathbf{d}$  where each index  $i$  contains the dot product between the counter-clockwise rotated mean query and the

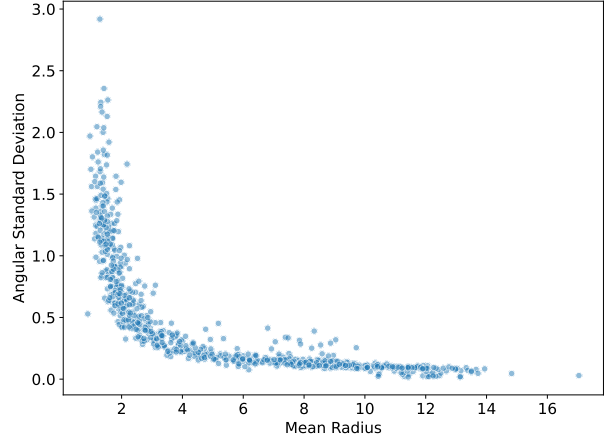


Figure 2. Circular angular standard deviation (Mardia & Jupp, 1999) vs radius for feature 12, other features follow a similar curve, where angular standard deviation decreases rapidly as radius increases.

mean key vector at a positional distance  $p$ . In the rest of this paper, when we mention "radius", we will be speaking about the rotary pair's mean vector's magnitude  $\|\bar{\mathbf{x}}_{\langle i \rangle}\|$ .

We find that rotary feature pairs with larger mean radius tend to have more stable angles with respect to the origin (Figure 2) so we expect this simplification to preserve the key patterns as the noisier a feature's angle is the less likely it is to contribute significantly to the dot product. However, some rotary feature vectors deviate significantly from the mean, often serving as attention sinks and this simplification will not capture these effects.

We calculate  $\mathbf{d}(p)$  for a range of distances and plot each component  $i$  as a function of  $p$  and their sum in Figure 5 and after scaling the sum  $D(p) = \sum_i d_i(p)$  by  $1/\sqrt{d_h}$  and applying the causal mask, we arrive at the resulting positional attention pattern. Comparing Figure 5 with Figure 4, we can see that  $D(p)$  recovers a focus on the first few tokens along the diagonal and quickly decays.

From this point on, we will use "feature" or "rotary feature" to refer to rotary feature pairs, since we will solely speak about rotary feature pairs.

#### 3.2. Rotary Offset Features and Bounds

What we find is that most of the outliers in rotary features are concentrated in rotary frequencies which never complete a full period. Furthermore, the ones that turn into large radii features within low frequencies tend to have a U-shaped contribution to  $D(p)$ , starting at a greater point than in the middle and often ending at a lesser point than they started. We call these features rotary offset features, and define them as:

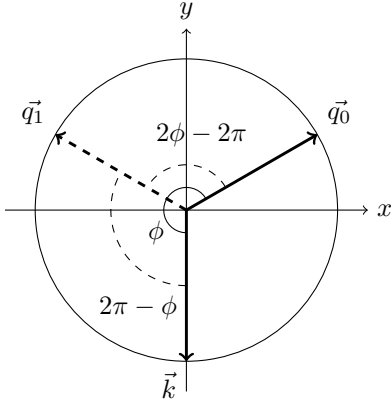


Figure 3. Query  $\vec{q}_0$  and key  $\vec{k}$  at an angle  $\phi > \pi$ . Using the relationship  $\cos\phi = \cos(2\pi - \phi)$ ,  $\phi - (2\pi - \phi)$  is the maximum rotation of  $q_0$  for it to return to same dot product,  $\vec{q}_1^T \vec{k} = \vec{q}_0^T \vec{k}$ , without exceeding the original dot product along the rotation.

**Definition 3.1.** A rotary feature  $i$  is a **rotary offset feature** if the dot product between mean query and mean key vectors are less than the starting dot product,  $d_i(p) < d_i(0)$ , for all positions less than or equal to the context length,  $p \leq p_{max}$ .

Using this definition, we can reason around the properties of rotary offset features and then test empirically whether the properties hold. Firstly, for the rotary offset feature to not return to the same value as at zero distance, the period of the rotation  $T = 2\pi/\theta$  must be greater than the context length  $p_{max}$ , giving us the upper bound on the rotary frequency:

$$\theta < \frac{2\pi}{p_{max}} \quad (15)$$

Secondly, we know that the initial angle between query and key needs to be  $\phi > \pi$ , since  $\cos\phi$  is increasing for  $[\pi, 2\pi]$  the rotary offset feature would be increasing above its initial value  $d_i(0)$  for some  $p \leq p_{max}$ . To arrive at a tighter lower bound for the initial angle, we need to use that  $\cos(2\pi - \phi) = \cos(\phi)$ , and the angular change  $\phi - (2\pi - \phi)$  gives us the angle at which the rotary offset feature returns to the same value as at zero distance (see Figure 3). This gives us the inequality  $p_{max}\theta \leq 2\phi - 2\pi$ , where the left hand side is the total rotation at the context length and the right hand side is the maximum change in angle to return to the value at zero distance. Rearranging this, we arrive at a lower bound for the query-key angle:

$$\phi > \pi + \frac{p_{max}\theta}{2} \quad (16)$$

These bounds only apply to rotary offset features, which tend to be the cause of the majority of outliers in low frequency features. It does not apply to other features such as

diagonal features which are typically high-frequency, fortunately these also tend to be of lower quantity and magnitude than rotary offset features as we will later observe (Figure 8).

## 4. Results

### 4.1. Model Selection

We focus our analysis on Phi-1 (Gunasekar et al., 2023), due to its low amount of rotary features which simplifies communication of results, and to a lesser extent DeepSeek-v2-lite (DeepSeek-AI et al., 2024), which has significant architectural differences to Phi-1, including multiheaded latent attention and a single rotary key for all rotary query heads, and Llama-2-7B (Touvron et al., 2023). The partial rotary embeddings should let us separate semantic from positional features and we should be able to observe the effects of the rotary positional embeddings more clearly.

Model	$d_h$	$r$	$p_{max}$	bias
Phi-1	64	32	2048	Yes
DeepSeek-v2-lite	192	64	163840	No
Llama-2-7B	128	128	4096	No

Table 1. Model architecture details showing head dimension ( $d_h$ ), rotary dimension ( $r$ ), context length ( $p_{max}$ ), and whether the linear projections for keys and queries have bias.

Throughout the paper, we use zero-based indexing for layers, heads, and features and will completely ignore non-rotary features. For all statistics and plots involving queries and keys, we analyze the data before applying rotary transformations, unless otherwise noted. We use rotary first with a sliced rotary implementation layout (as typical by transformers implementation (Wolf et al., 2020)), we reorder DeepSeek’s activations<sup>2</sup> to follow this layout as well.

We use the configured max position embeddings of models,  $p_{max}$ , as a proxy for trained context length. This assumes that the models were trained with this sequence length.

### 4.2. Single Head Analysis

We begin our analysis with a single head in Phi-1. We will later show that the patterns are in many other heads and layers, followed by an analysis showing the patterns exist across different architectures and language models.

**Cyclic Rotary Features** Various positional attention patterns can be constructed using the rotary features that complete several cycles during the context length, as they form a combination of sinusoidal functions of various amplitudes and frequencies. For instance, in heads with banded atten-

<sup>2</sup>DeepSeek-V2-Lite has rotary last interleaved layout

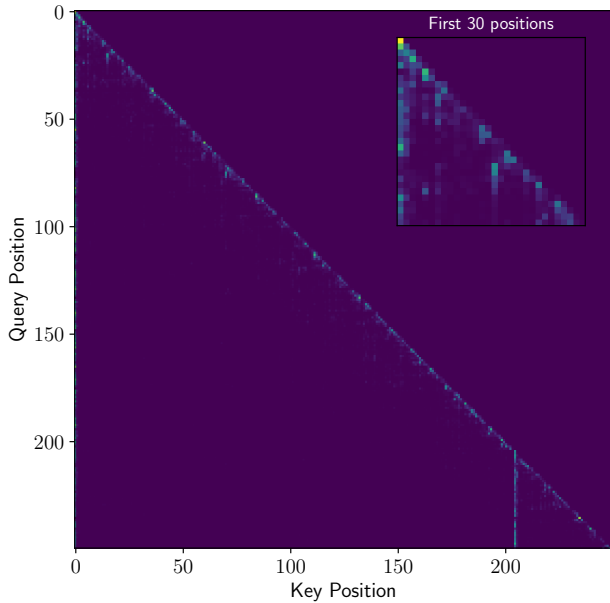


Figure 4. Attention pattern for a single head showing characteristic sub-diagonal structure and two attention sinks (position 0 and 204).

tion patterns, as in the head we have chosen to study, Figure 4, uses multiple low-to-mid frequency components (as seen in the decomposition in Figure 5) to build up a maximum attention score at distance zero and one and then quickly decays, forming a banded diagonal pattern.

**Partial Cycle Rotary Features** Some of the most consistent outlier features across heads and layers (and as we’ll see, across different models) are the features that go through exactly a full period or less of the RoPE rotations during the model’s context length. These tend to be selected to ensure the attention score does not return to the same value as at early distances. See Figure 5 for an example where feature 12 starts at a large negative value.

Rotary offset features are the ones that create the bands of large magnitudes in the query and key plots in Figure 1. In Phi-1, these bands are formed around feature 12. For the head we have selected for analysis, feature 12 is also the feature with greatest radius of the head’s rotary features. In Figure 7, we see that the feature has a large radius in both query and key and maintains consistent angles with respect to the origin (with some exceptions discussed later). The angle between the query and key vectors for feature 12 tend to form an angle  $\phi_{12}$  which would result in a significant negative dot product. We also show the full rotation throughout the context length, which covers less than half a full period. This head is in no way unique and the angle between query and key are surprisingly similar across heads and layers for feature 12 when the radius is large (see Figure 8).

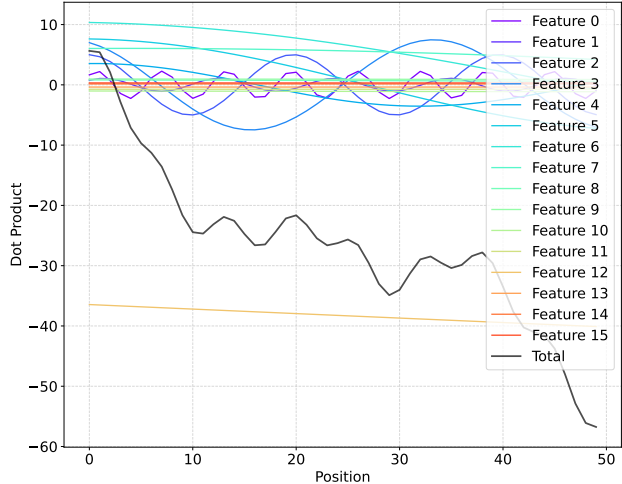


Figure 5. Each rotary feature’s dot product component of  $\mathbf{d}(p)$  for a range of positions  $p$  and the total sum of the components showing the unnormalized attention score as distance increases. Feature 12 starts at about  $-35$  at  $p = 0$ . The positional attention pattern focuses on the first three tokens. The reconstructed positional attention pattern is in the Appendix, Figure 10.

To better understand the feature’s contribution to the dot product  $D(p)$ , we study what happens when we exclude this feature from  $D(p)$ . In Figure 6, we see that at short distances ( $p \lesssim 50$ ) excluding feature 12, just shifts the curve up, which since softmax is invariant to adding a constant to all inputs,  $\text{softmax}(\mathbf{x} + c) = \text{softmax}(\mathbf{x})$ , would result in the same attention pattern. However, at longer distances there is a large difference in  $D(p)$ , at many points where the other features would add up to being close to values at the start, feature 12 has shifted them down, making their contribution to the attention score negligible. At the end,  $d_{12}(p_{max})$  is closing in on its value at the start, but the other features,  $d_{0:15} \setminus 12$ , do not peak at the same time as at the start which results in a relatively much lower attention score. In other words, without feature 12, the attention pattern would look very different at longer distances and would at certain intervals attend tokens that are distant.

**Attention sinks** In Figure 7, we also see that Feature 12 plays a role in which tokens are selected as attention sinks in this head, with `<end_of_text>` and the first `\n` being selected. In Figure 7, we see that the head makes use of the low frequency rotary feature pair and aligns the keys of the attention sinks to the queries’ mean angle resulting in a positive dot product across positions, it then proceeds to put all other keys at angles from the queries’ mean angle which result in consistently smaller dot product for the other keys, leading to a large amount of attention on the attention sinks leading to the typical vertical attention pattern, as seen at position 0 and 204 in Figure 4.

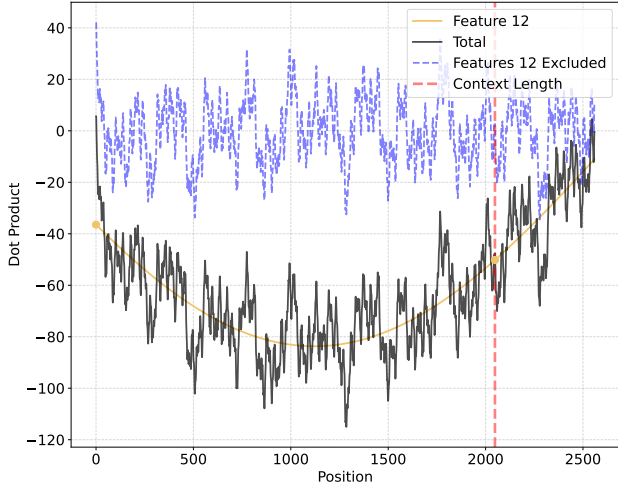


Figure 6.  $D(p)$  for positions 0-2560 (512 past the context length of Phi-1) with the addition of a line for what happens when we exclude feature 12 and feature 12 without other features. Feature 12 never completes a cycle. Figure 7 top plot shows the corresponding rotation during the context length.

### 4.3. Model Analysis

#### 4.3.1. PHI-1

**General observations** We observe that many of the relationships in the head we just analyzed are present across other layers and heads in Figure 8. Large radii features tend to be at certain angles  $\phi_i$ . It can be observed for Phi-1 that most of them are at low frequencies, with the exception of feature 0, which is a cyclic rotary feature. For Feature 0 the largest radii heads are located around  $\phi = 1rad$  which is equal to the angular step per position,  $\theta_0 = 1$ , so the query and key will tend to maximise their dot product at a distance of one, suggesting these are the features that select for the previous token.

**Rotary offset features cutoff** For feature 12, we see a similar angle as we did in our single head analysis and that it exists in many heads and across layers of the network. There exists heads with feature 11-15 with much larger radii than for feature 10 and below. For Phi-1’s feature 10, we calculate an upper bound of  $p_{max}\theta_{10} = 6.38$ , which exceeds  $2\pi$ , this indicates that feature 10 and any higher frequency rotary features would be unsuitable as rotary offset features since they go through more than a full period in the context length. We observe a sharp increase in maximum radii between features 10 and 11, aligning with our predictions about which features can effectively serve as rotary offset features.

**Initial angle of rotary offset features** We visualize the lower bounds in Figure 8. By inspection, the model seems

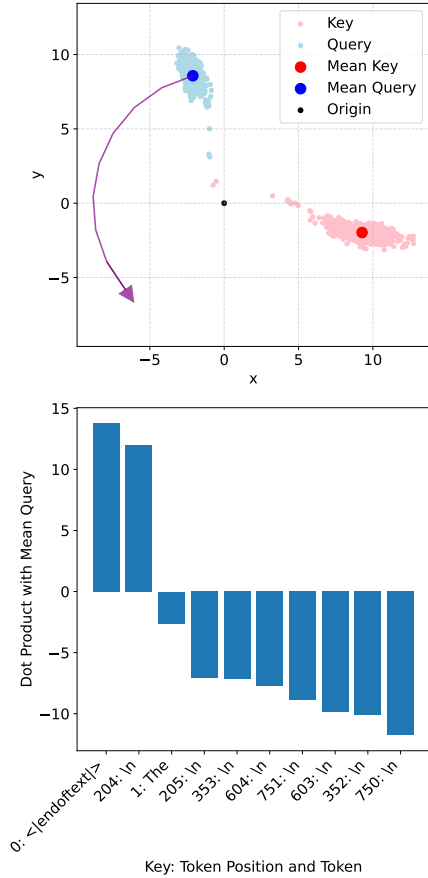


Figure 7. Feature 12’s keys and queries are shown, with their respective means. The curved line shows the trajectory of the mean query rotated with frequency  $\theta_{12}$  across the network’s context length,  $p_{max}$ . The query and key means maintain angles throughout that yield a consistently negative dot product. The two pink dots just above the origin are the attention sink keys, which align with the query angle. These are the only two tokens (out of over 800, bottom plot for top 10) that produce positive dot products, causing them to receive a large proportion of the attention weight.

to have learnt and agree with these bounds and the majority of large radii heads maintain angles above or very close to the lower bound for each feature.

#### 4.3.2. METRICS ACROSS MODELS

DeepSeek-V2-Lite and Llama-2-7b also have rotary offset features, similarly to Phi-1, despite their different architectures. Table 2 presents the recall metrics for both upper and lower bounds across our analyzed models. For the upper bound, we find that most outliers exist in the rotary offset features, with over 90% of the outlier features being in potential rotary offset features selected by the upper bound. The lower bound, despite covering only approximately 35% of possible angles within roughly 30% of all features, successfully captures the majority of outlier features across all

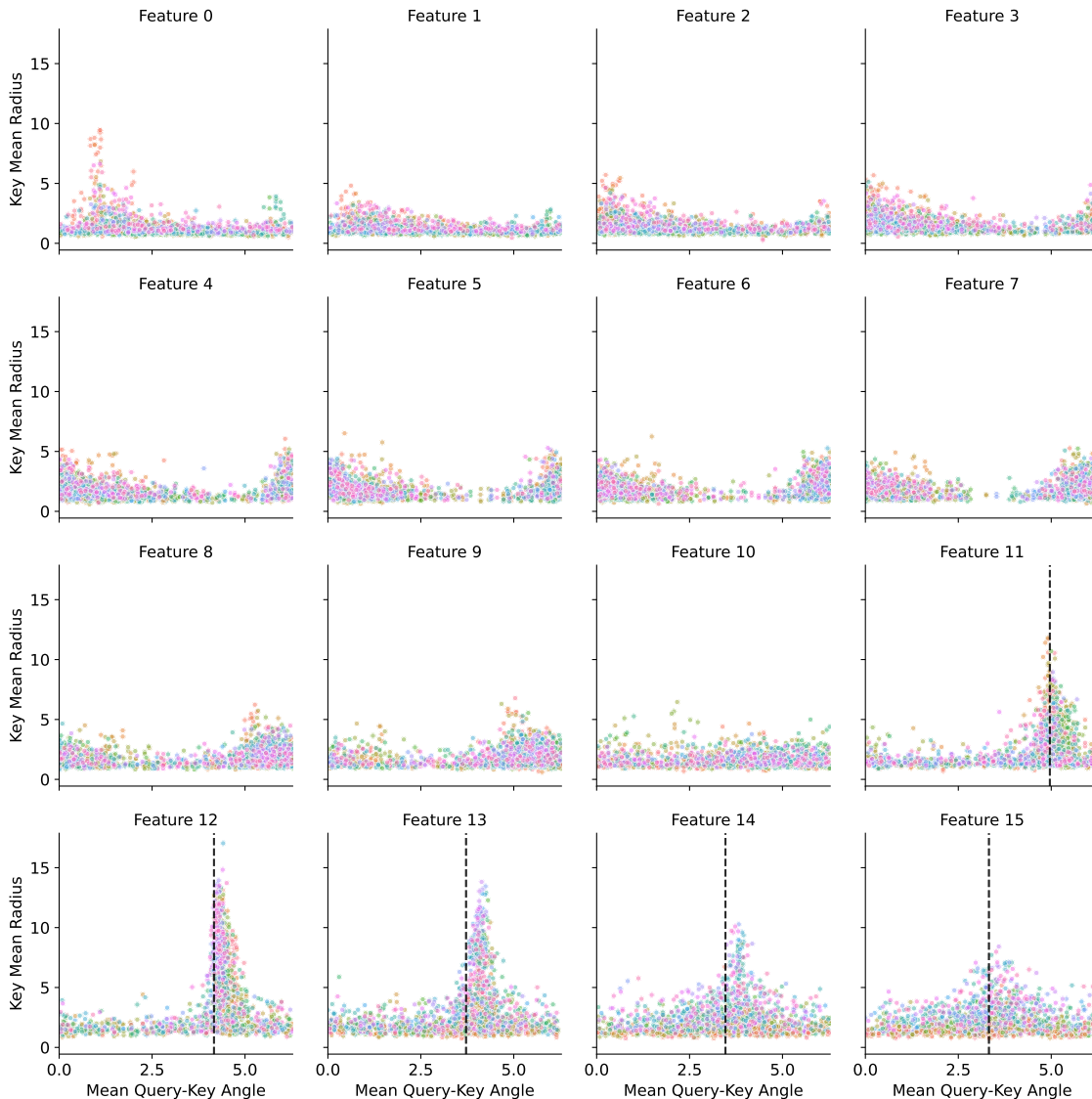


Figure 8. Mean radius of rotary key features plotted against the angle between mean query and mean key for each layer (colored) and head of Phi-1 (768 datapoints for each feature). Black dashed line for feature 11-15 are the soft lower bounds for the angle  $\phi_i$  for each feature to serve as a rotary offset feature. Any feature without a dashed line are outside the bounds.

three models. Visual evidence in Figures 8 (and Figure 11 for DeepSeek, in Appendix) further supports this finding, showing clear clustering of large radius features around our predicted lower bounds. This clustering provides strong evidence that our derived lower bounds accurately identify effective rotary offset features and that they tend to contain large magnitude features. Relaxing our lower bound by 0.1 rad or  $\sim 6^\circ$  we see that the recall for the lower bound increases, indicating that large amounts of outlier features are also just below the lower bound.

### 5. Discussion

Our predictions about the behaviour of rotary offset features and the empirical results from our bounds suggest that the main drivers for outlier features in low-frequency rotary features are rotary offset features. The rotary pairs of these features correspond to the two high-norm bands seen in Figure 1.

### 6. Related Work

(Chen et al., 2024; Liu et al., 2024a) studies length generalization in RoPE and hypothesizes that low-frequency

**Rotary Outliers and Rotary Offset Features in Large Language Models**

Model	Features	%ROF	Mean LB	Radius	Outlier Feat.	UB Recall	LB / LB-0.1 Recall
Phi-1	12288	31%	3.93	6	634	0.97	0.88 / 0.94
				9	252	0.99	0.94 / 0.98
				12	46	1.00	1.00 / 1.00
Llama-2-7b	65536	28%	4.19	6	1242	0.95	0.72 / 0.84
				9	730	1.00	0.79 / 0.94
				12	180	1.00	0.79 / 0.96
DeepSeek-V2-Lite <sup>†</sup>	13824	28%	4.26	6	640	0.92	0.66 / 0.84
				9	464	1.00	0.68 / 0.94
				12	352	1.00	0.74 / 0.97

Table 2. Metrics for Phi-1 and Llama-2-7b models for keys, showing the number of rotary features, percentage of rotary features that could be selected as rotary offset features (%ROF), mean lower bound for the angles  $\phi_i$  across all the rotary offset features, the radius for defining outlier features, the number of outlier features defined by the outlier radius, recall for the upper bound of outlier features, and the recall of outlier features for the lower bound / relaxed lower bound (by 0.1 rad or  $\sim 6^\circ$ ) for the mean query-key angle. <sup>†</sup> For DeepSeek-V2-Lite, note that the rotary keys in these statistics are repeated 16 times since each rotary key is matched to 16 rotary queries.

features are unable to generalize to lengths beyond the context length. They derive an upper bound for the frequency of these features which turns out to be the same as the upper bound for our rotary offset features. We independently discovered this upper bound during our research on rotary outlier features and show how it can instead be applied to predict which rotary frequencies are likely to contain outlier activations.

(Barbero et al., 2024) performs an in-depth analysis of RoPE. They also note that high frequency rotary feature pairs are used to create previous token (sub-diagonal) heads and note heavy use of low-frequency components in Gemma.

(Jin et al., 2025) studies massive values in large language models and found independently and concurrently to us massive values in queries and keys, that they are present in models using RoPE, and that they are found in rotary feature pairs.

Recent work has identified attention sinks (Xiao et al., 2024) as a key mechanism in language models, where certain tokens (typically beginning of the sequence and semantically unimportant tokens) persistently receive high attention scores across many attention heads. Our analysis reveals the rotary offset features as one mechanism of how attention sinks are consistently selected for across positions. (Gu et al., 2024) also notes that attention sinks emerge when the cosine between queries and keys is positive and large. We show how this works on an individual query-key level and how it relates to the rotary offset features.

(Liu et al., 2024b) studies how to improve kv-cache quantization. They note that high-norm channels in keys are not present in the value vectors. They choose to employ asymmetric channel-wise quantization for keys, among other techniques, to reduce the impact of these high-norm channels on the model’s performance after quantization.

## 7. Conclusion

We have presented a detailed analysis of rotary features in language models, revealing consistent patterns across architectures and scales. Our analysis reveals several key findings about how transformers utilize rotary positional embeddings:

First, we demonstrate that certain rotary feature pairs consistently emerge as outliers with large radii across different models and architectures. These outliers serve specific positional attention functions - low frequency features enable rotary offset features while high frequency features create precise positional patterns like sub-diagonal attention.

Second, we derive bounds that explain why lower frequency rotary features can effectively implement rotary features that offset the attention score with distance and what angle their rotary pairs’ queries and keys tend to be above. This matches empirical observations of where outlier features emerge.

We hope the derived bounds, the insights and the analysis presented in this paper can help further the understanding of models using rotary positional embeddings, lead to improvements in the frequency selection of rotary features, and potentially inform the development of improved quantization algorithms for language models using rotary embeddings.

## Impact Statement

This paper advances understanding of language model architectures. The insights may enable more efficient implementations through improved quantization, potentially reducing computational costs and environmental impact of large language model deployment.

## References

- Barbero, F., Vitvitskiy, A., Perivolaropoulos, C., Pascanu, R., and Veličković, P. Round and round we go! what makes rotary positional encodings useful? *arXiv preprint arXiv:2410.06205*, 2024.
- Chen, Y., Lv, A., Luan, J., Wang, B., and Liu, W. Hope: A novel positional encoding without long-term decay for enhanced context awareness and extrapolation. *arXiv preprint arXiv:2410.21216*, 2024.
- DeepSeek-AI, Liu, A., Feng, B., Wang, B., Wang, B., Liu, B., Zhao, C., Dengr, C., Ruan, C., Dai, D., Guo, D., Yang, D., Chen, D., Ji, D., Li, E., Lin, F., Luo, F., Hao, G., Chen, G., Li, G., Zhang, H., Xu, H., Yang, H., Zhang, H., Ding, H., Xin, H., Gao, H., Li, H., Qu, H., Cai, J. L., Liang, J., Guo, J., Ni, J., Li, J., Chen, J., Yuan, J., Qiu, J., Song, J., Dong, K., Gao, K., Guan, K., Wang, L., Zhang, L., Xu, L., Xia, L., Zhao, L., Zhang, L., Li, M., Wang, M., Zhang, M., Zhang, M., Tang, M., Li, M., Tian, N., Huang, P., Wang, P., Zhang, P., Zhu, Q., Chen, Q., Du, Q., Chen, R. J., Jin, R. L., Ge, R., Pan, R., Xu, R., Chen, R., Li, S. S., Lu, S., Zhou, S., Chen, S., Wu, S., Ye, S., Ma, S., Wang, S., Zhou, S., Yu, S., Zhou, S., Zheng, S., Wang, T., Pei, T., Yuan, T., Sun, T., Xiao, W. L., Zeng, W., An, W., Liu, W., Liang, W., Gao, W., Zhang, W., Li, X. Q., Jin, X., Wang, X., Bi, X., Liu, X., Wang, X., Shen, X., Chen, X., Chen, X., Nie, X., Sun, X., Wang, X., Liu, X., Xie, X., Yu, X., Song, X., Zhou, X., Yang, X., Lu, X., Su, X., Wu, Y., Li, Y. K., Wei, Y. X., Zhu, Y. X., Xu, Y., Huang, Y., Li, Y., Zhao, Y., Sun, Y., Li, Y., Wang, Y., Zheng, Y., Zhang, Y., Xiong, Y., Zhao, Y., He, Y., Tang, Y., Piao, Y., Dong, Y., Tan, Y., Liu, Y., Wang, Y., Guo, Y., Zhu, Y., Wang, Y., Zou, Y., Zha, Y., Ma, Y., Yan, Y., You, Y., Liu, Y., Ren, Z. Z., Ren, Z., Sha, Z., Fu, Z., Huang, Z., Zhang, Z., Xie, Z., Hao, Z., Shao, Z., Wen, Z., Xu, Z., Zhang, Z., Li, Z., Wang, Z., Gu, Z., Li, Z., and Xie, Z. Deepseek-v2: A strong, economical, and efficient mixture-of-experts language model, 2024. URL <https://arxiv.org/abs/2405.04434>.
- Dettmers, T., Lewis, M., Belkada, Y., and Zettlemoyer, L. Gpt3. int8 (): 8-bit matrix multiplication for transformers at scale. *Advances in neural information processing systems*, 35:30318–30332, 2022.
- Gu, X., Pang, T., Du, C., Liu, Q., Zhang, F., Du, C., Wang, Y., and Lin, M. When attention sink emerges in language models: An empirical view, 2024. URL <https://arxiv.org/abs/2410.10781>.
- Gunasekar, S., Zhang, Y., Aneja, J., Mendes, C. C. T., Giorno, A. D., Gopi, S., Javaheripi, M., Kauffmann, P., de Rosa, G., Saarikivi, O., Salim, A., Shah, S., Behl, H. S., Wang, X., Bubeck, S., Eldan, R., Kalai, A. T., Lee, Y. T., and Li, Y. Textbooks are all you need, 2023. URL <https://arxiv.org/abs/2306.11644>.
- Jin, M., Mei, K., Xu, W., Sun, M., Tang, R., Du, M., Liu, Z., and Zhang, Y. Massive values in self-attention modules are the key to contextual knowledge understanding, 2025. URL <https://arxiv.org/abs/2502.01563>.
- Liu, X., Yan, H., An, C., Qiu, X., and Lin, D. Scaling laws of roPE-based extrapolation. In *The Twelfth International Conference on Learning Representations*, 2024a. URL <https://openreview.net/forum?id=J07k0SJ5V6>.
- Liu, Z., Yuan, J., Jin, H., Zhong, S., Xu, Z., Braverman, V., Chen, B., and Hu, X. Kivi: A tuning-free asymmetric 2bit quantization for kv cache. *arXiv preprint arXiv:2402.02750*, 2024b.
- Mardia, K. V. and Jupp, P. E. *Directional Statistics*. Wiley Series in Probability and Statistics. Wiley, Chichester, 1999. doi: 10.1002/9780470316979.
- Su, J., Ahmed, M., Lu, Y., Pan, S., Bo, W., and Liu, Y. Roformer: Enhanced transformer with rotary position embedding. *Neurocomputing*, 568:127063, 2024.
- Touvron, H., Martin, L., Stone, K., Albert, P., Almahairi, A., Babaei, Y., Bashlykov, N., Batra, S., Bhargava, P., Bhosale, S., Bikel, D., Blecher, L., Ferrer, C. C., Chen, M., Cucurull, G., Esiobu, D., Fernandes, J., Fu, J., Fu, W., Fuller, B., Gao, C., Goswami, V., Goyal, N., Hartshorn, A., Hosseini, S., Hou, R., Inan, H., Kardas, M., Kerkez, V., Khabsa, M., Kloumann, I., Korenev, A., Koura, P. S., Lachaux, M.-A., Lavril, T., Lee, J., Liskovich, D., Lu, Y., Mao, Y., Martinet, X., Mihaylov, T., Mishra, P., Molybog, I., Nie, Y., Poulton, A., Reizenstein, J., Rungta, R., Saladi, K., Schelten, A., Silva, R., Smith, E. M., Subramanian, R., Tan, X. E., Tang, B., Taylor, R., Williams, A., Kuan, J. X., Xu, P., Yan, Z., Zarov, I., Zhang, Y., Fan, A., Kambadur, M., Narang, S., Rodriguez, A., Stojnic, R., Edunov, S., and Scialom, T. Llama 2: Open foundation and fine-tuned chat models, 2023. URL <https://arxiv.org/abs/2307.09288>.
- Vaswani, A. Attention is all you need. *Advances in Neural Information Processing Systems*, 2017.
- Wolf, T., Debut, L., Sanh, V., Chaumond, J., Delangue, C., Moi, A., Cistac, P., Rault, T., Louf, R., Funtowicz, M., Davison, J., Shleifer, S., von Platen, P., Ma, C., Jernite, Y., Plu, J., Xu, C., Le Scao, T., Gugger, S., Drame, M., Lhoest, Q., and Rush, A. Transformers: State-of-the-art natural language processing. In Liu, Q. and Schlangen, D. (eds.), *Proceedings of the 2020 Conference on Empirical Methods in Natural Language Processing: System Demonstrations*, pp. 38–45, Online, October

2020. Association for Computational Linguistics. doi: 10.18653/v1/2020.emnlp-demos.6. URL <https://aclanthology.org/2020.emnlp-demos.6/>.

Xiao, G., Tian, Y., Chen, B., Han, S., and Lewis, M. Efficient streaming language models with attention sinks, 2024. URL <https://arxiv.org/abs/2309.17453>.

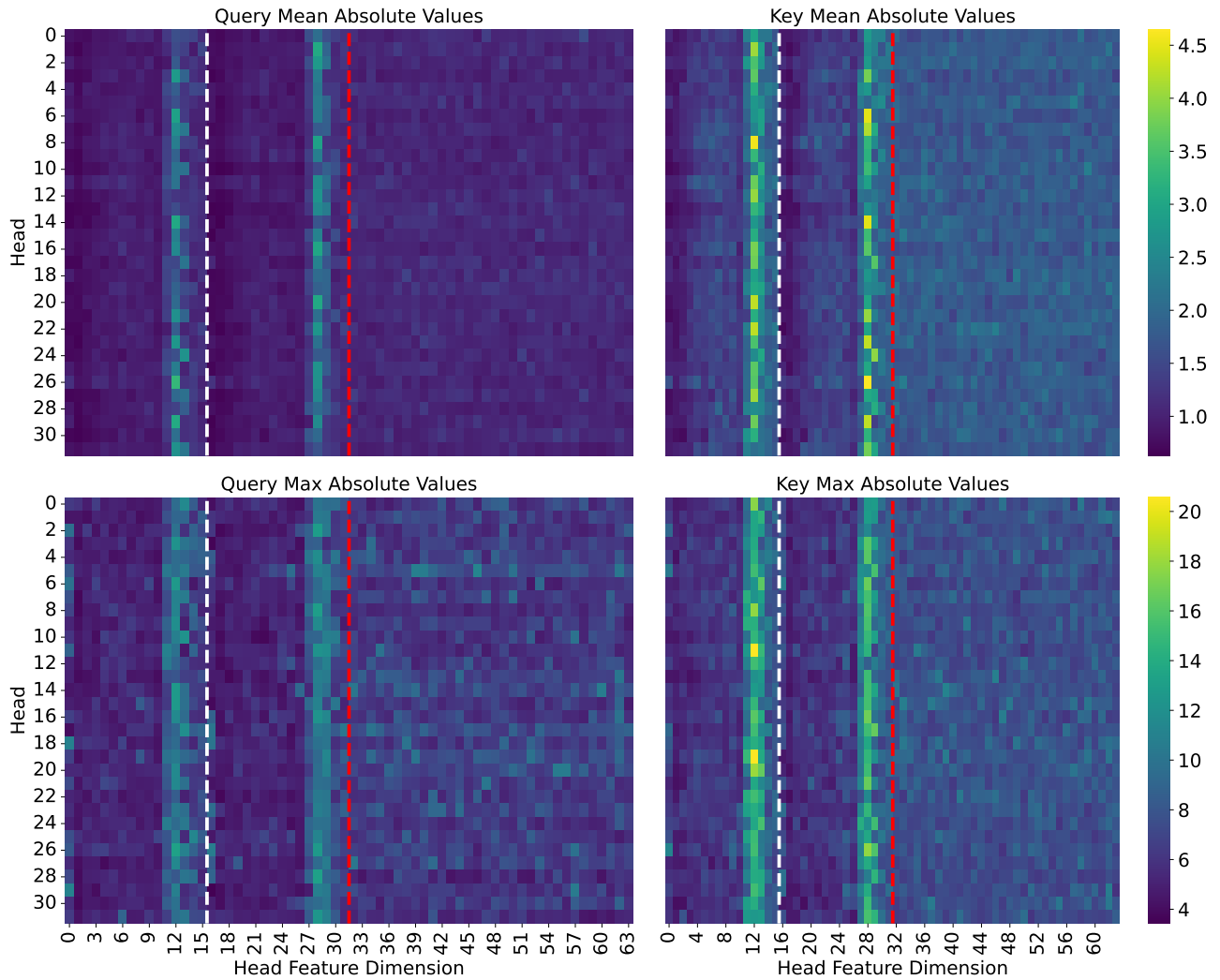


Figure 9. Query and key magnitudes prior to rotation in Phi-1. The white dashed line separates rotary (left) from non-rotary (right) features, we further separate the first dimensions of the rotary pairs (left) from the second dimensions (right) with a red dashed line. The bands of large absolute values are located at the pair of dimensions that are rotated by the same low frequency in a sliced rotary implementation layout.

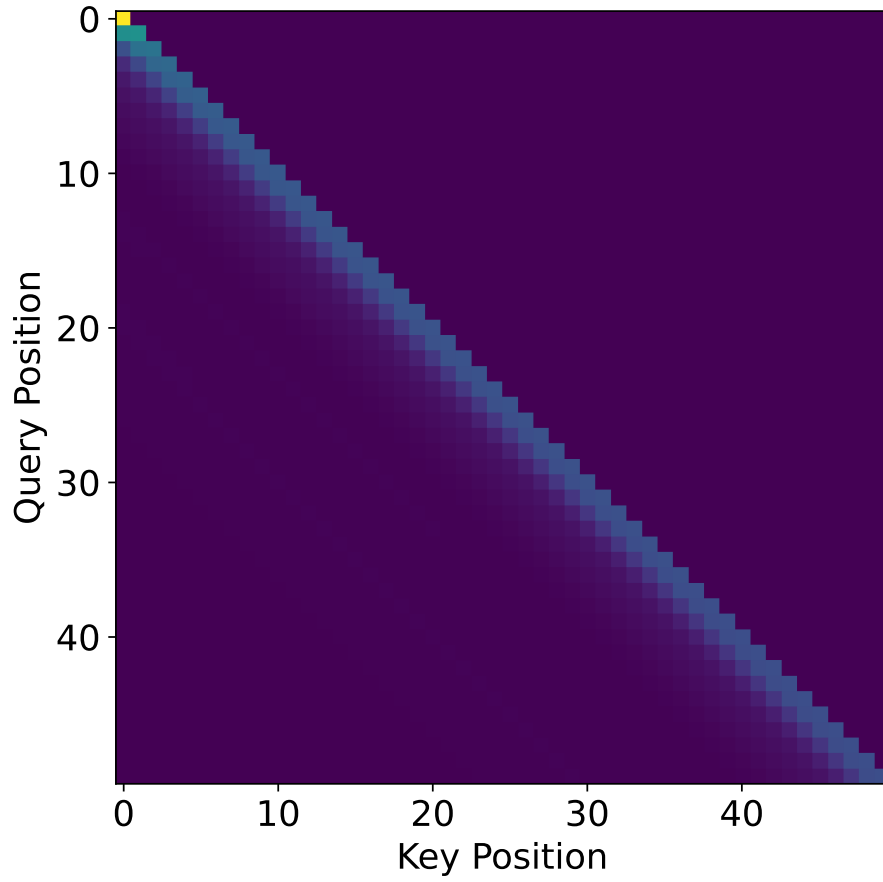


Figure 10. Positional attention pattern resulting from applying scaling, masking and softmax to  $\Sigma_i d_i(p)$  that is visualized as the total in Figure 5.

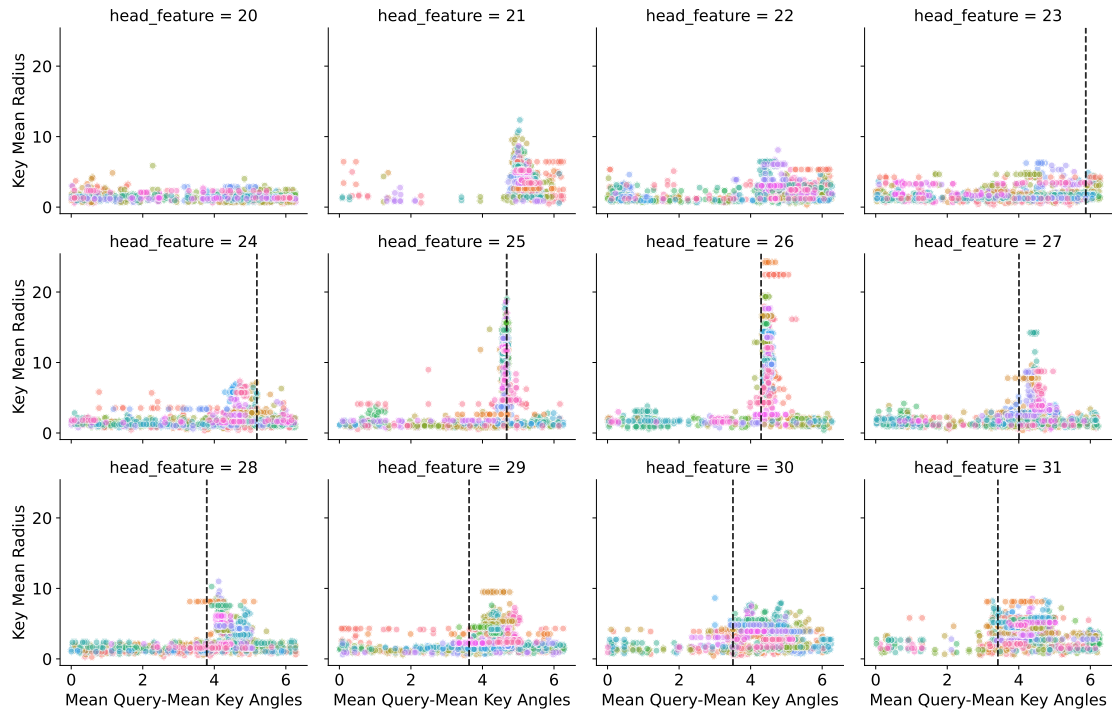


Figure 11. DeepSeek-V2-Lite: Mean radius of keys plotted against the angle between mean query and mean key for each layer (colored) and head for the last 12 rotary features. Black dashed lines for feature 23-31 are the lower bounds for the angle  $\phi_i$  for each feature to serve as a rotary offset feature. Any feature without a dashed line are outside the bounds. The rotational keys are repeated 16 times to match the queries, so there are 16 times as many datapoints as there are actual rotational keys. We do note a single feature, feature 21, which is a cyclic rotary feature which has some values approaching that of the outliers.